

Optical properties of a spherical 2D electron gas in the presence of a uniform magnetic field

Ali Ihsan Goker* and Peter Nordlander†

Department of Physics and Department of Electrical and Computer Engineering

Rice Quantum Institute

M.S. 61, Rice University

Houston, TX 77251-1892, USA

Abstract

Using the RPA, we calculate the plasmon frequencies of an electron gas on a two-dimensional spherical surface in the presence of a weak magnetic field. We show that the magnetic field results in a coupling between electronic states with different angular momentum numbers. This coupling results in a blueshift of the dipolar plasmon resonance with increasing magnetic field. We also investigate how the plasmon energies vary as a function of the surface density of electrons and radius of the sphere.

Keywords: Zeeman effect, RPA, Magnetoplasmon, Nanophotonics

*email: agoker@rice.edu

†email: nordland@rice.edu

I. INTRODUCTION

Metallic shell structures are of considerable theoretical and experimental interest because of their unusual electronic and optical properties.[1, 2, 3, 4, 5] In recent years, it has been possible to manufacture spherical shaped nanostructures ranging from fullerene size to nano-sized objects such as SiO_2 balls in opals [6], nanoshells [7] and multielectron bubbles [8, 9]. The motion of charged particles on such spheres with constant magnetic field along a given axis of the sphere has been studied previously.[10, 11, 12, 13] The energy spectrum has been calculated and the thermodynamical properties, such as magnetization and susceptibility, have been studied rigorously.

In the case of multielectron bubbles, the electrons move freely in the direction tangential to the spherical helium surface, therefore they effectively form a spherical two-dimensional electron gas. A S2DEG can also be realized in charge droplets [14] and in doped semiconductor particles if carriers accumulate in a surface layer.[15] In previous work, the many-body properties of such a system were investigated using the random-phase approximation, and multipole excitation modes of the S2DEG have been calculated [16] and the angular-momentum dependent dielectric function of the S2DEG has been derived.[17] Also, an exact solution for this system in weak and strong magnetic fields was developed.[18]

Motivated by these recent works, we will analyze the optical response of the S2DEG in the presence of a weak uniform magnetic field along a given axis. In this regime, we can treat the system perturbatively. We investigate how the dipolar plasmon energy is affected as the magnetic field or the density of electrons is changed. We hope to provide insight as to how these magnetoplasmons can be useful in developing nanophotonics applications.

II. THEORY

In this section, we will develop the theoretical framework within which we treated the S2DEG. We will first describe the effect of a weak magnetic field on the ground state of the electron gas. We will then use this result to obtain the response properties of the S2DEG using linear response theory.

The system under investigation is electrons constrained to the surface of a sphere of radius r_0 in the Landau gauge. Throughout this paper, we will assume closed shell configuration

for the ground state of the electron gas, i.e. all the angular momentum states, until the Fermi level are fully occupied with two projections of spin. The Fermi angular momentum number L_F determines the number of electrons in the system by

$$N = 2(L_F + 1)^2 \quad (1)$$

and the surface charge density is

$$\nu = \frac{N}{4\pi r_0^2}. \quad (2)$$

We will use a confining potential of the form

$$V(r) = \begin{cases} 0 & \text{for } r_0 < r < r_0 + \delta r \\ \infty & \text{otherwise} \end{cases} \quad (3)$$

in the Schrodinger equation. If we assume $\delta r \ll r_0$, this potential describes a shell with infinitesimal thickness, thus the radial and angular variables of the Schrodinger equation can be separated. If the Fermi level lies below the first excited level of the radial component of the wave function, we can ignore the radial component and put $r = r_0$ in the remaining angular part of the Hamiltonian H_Ω . This requires $\delta r \leq \nu^{-1/2}$ and, if satisfied, means that we are dealing with an effectively two-dimensional system. Now, we apply a uniform magnetic field along z axis of the sphere ($\theta = 0$). Since the system has rotational symmetry, an eigenfunction can be written as $\Psi(\theta, \phi) = \Theta(\theta) \exp(im\phi)$, where $m\hbar$ is the eigenvalue of \hat{L}_z . The angular part of the Schrodinger equation in atomic units takes the form

$$\frac{\partial}{\partial \zeta}(1 - \zeta^2) \frac{\partial \Theta}{\partial \zeta} + [\varepsilon - 2mp - \frac{m^2}{1 - \zeta^2} - p^2(1 - \zeta^2)]\Theta = 0 \quad (4)$$

upon introducing $\zeta = \cos\theta$, the dimensionless energy $\varepsilon = 2r_0^2 E$ and the number of flux quanta p encircled by the sphere which is given by

$$p = \frac{\pi B r_0^2}{\Phi_0}, \quad (5)$$

where $\Phi_0 = \frac{2\pi}{e} = 2 \times 10^{-15} T m^2$ is the flux quantum.

The above equation is the well-known spheroidal differential equation.[19, 20] In the absence of magnetic field, this equation reduces to the standard free rotator problem in quantum mechanics and the wave functions are the spherical harmonics. In the presence of weak magnetic field, however, one is able to develop a perturbation theory around the

initial wave functions as long as $p^2 \leq 4l$ to get a series of Zeeman-split $2(2l + 1)$ states with energy eigenvalues [18]

$$\varepsilon_{lm\sigma}(p) = l(l + 1) + 2pm + \frac{p^2}{2} \left[1 + \frac{m^2}{l^2} \right] + \frac{p^2}{l} + \frac{2\Phi_0}{137\pi} p\sigma + O(p^4) \quad (6)$$

and normalized wave functions

$$\Psi_{lm}(p, \Omega) = \frac{Y_{lm}(\Omega) + \frac{p^2}{l} Y_{l+2,m}(\Omega) + \frac{p^2}{l} Y_{l-2,m}(\Omega)}{\sqrt{1 + \frac{2p^4}{l^2}}} + O(p^4), \quad (7)$$

where Ω denotes the spherical angles $\Omega = \{\theta, \phi\}$ and (l, m) represent the angular momentum state. In Eq. (6), the last term represents the contribution from the spin degrees of freedom and σ denotes the projection of the spin. This term is much smaller than the others, and will be neglected in the following.

Our aim in this paper is to use the above perturbed energy eigenvalues and wavefunctions to calculate the dielectric response function using the random phase approximation(RPA). We will investigate the behaviour of the optically active dipolar plasmon energy in presence of the magnetic field. Using second quantization, the surface density operator can be expressed as

$$\hat{n}_e(p, \Omega) = \sum_{l=0}^{\infty} \sum_{m=-l}^l \sum_{l'=0}^{\infty} \sum_{m'=-l'}^{l'} \Psi_{l,m}^*(p, \Omega) \Psi_{l',m'}(p, \Omega) \hat{c}_{l,m}^\dagger \hat{c}_{l',m'}, \quad (8)$$

where $\Psi_{l',m'}(p, \Omega)$ refers to Eq. (7). $\hat{c}_{l,m}^\dagger$ is the fermion creation operator which creates an electron in the state $\Psi_{l,m}(p, \Omega)$ and $\hat{c}_{l,m}$ is the fermion destruction operator which destroys an electron in the single particle state $\Psi_{l,m}(p, \Omega)$.

We can also expand the density operator $\hat{n}_e(p, \Omega)$ in spherical harmonics which is a complete orthonormal set as

$$\hat{n}_e(p, \Omega) = \sum_{l=0}^{\infty} \sum_{m=-l}^l \hat{\rho}_e(p, l, m) Y_{lm}^*(\Omega). \quad (9)$$

If we invert this equation by using the orthogonality relation of the spherical harmonics and insert Eq.(8) for $\hat{n}_e(p, \Omega)$, we obtain the the spherical components of the density operator as

$$\hat{\rho}_e(p, l, m) = \sum_{L=0}^{\infty} \sum_{M=-L}^L \sum_{l'=0}^{\infty} \sum_{m'=-l'}^{l'} \left[\int Y_{lm}(\Omega) \Psi_{L,M}^*(p, \Omega) \Psi_{l',m'}(p, \Omega) d\Omega \right] \hat{c}_{L,M}^\dagger \hat{c}_{l',m'}, \quad (10)$$

where (l', m') and (L, M) denote the initial and final angular momentum states respectively. The quantum numbers (l, m) refers to the excitation connecting the initial and final states.

The interaction of the electrons moving on the surface of the sphere is entirely described by the Coulomb potential energy in the Hamiltonian and this term is unaffected by the presence of the magnetic field. In second quantization, it is given by

$$\hat{H}_{Coulomb} = \sum_{l_1, m_1} \sum_{l_2, m_2} \sum_{l, m} (-1)^m v(l) \times \hat{c}_{(l_1, m_1) \otimes (l, -m)}^\dagger \hat{c}_{(l_2, m_2) \otimes (l, m)}^\dagger \hat{c}_{l_2, m_2} \hat{c}_{l_1, m_1}, \quad (11)$$

where $v(l, r_0) = \frac{1}{2r_0(2l+1)}$ is the interaction amplitude and the operator $\hat{c}_{(l_1, m_1) \otimes (l, -m)}^\dagger$ creates an electron in a state which results from the combination of two states with (l_1, m_1) and $(l, -m)$. [17] The Coulomb interaction term represents the exchange of a virtual photon with (l, m) between two electrons in initial states with (l_1, m_1) and (l_2, m_2) .

In linear response theory, an induced electron density $\rho_{ind}(p, \Omega, \omega)$ is generated when an external field $V_{ext}(\Omega, \omega)$ which couples to the electron density is applied. Its spherical components can be written as

$$\rho_{ind}(p, l, m, \omega) = V_{ext}(l, m, \omega) D_R(p, l, m, \omega), \quad (12)$$

where $D_R(p, l, m, \omega)$ is the retarded density-density Green's function. It is derived from the density-density Green's function:

$$D(p, l, m, t) = i \langle \Psi_0 | \tau \hat{\rho}_e(p, l, m, t) \hat{\rho}_e(p, l, -m, t) | \Psi_0 \rangle, \quad (13)$$

where τ is the time ordering operator, expectation value is taken with respect to the many body ground state and the interaction picture is used in spherical components of the density operator to bring in time dependence. We can now obtain the Lindhard or independent electron response function $D_R^0(p, l, m, \omega)$ easily by replacing the wavenumber with the angular momenta in the standard Green's function methods. After making use of analytical continuation, the result takes the form:

$$D_R^0(r_0, p, l, m, \omega) = \sum_{l', m'} \sum_{L, M} n(l', m') (1 - n(L, M)) \left| \int Y_{l, m}(\Omega) \Psi_{L, M}^*(p, \Omega) \Psi_{l', m'}(p, \Omega) d\Omega \right|^2 \times \left(\frac{1}{\omega + \frac{\varepsilon_{l', m'}(p) - \varepsilon_{L, M}(p)}{2r_0^2} + i\eta} - \frac{1}{\omega + \frac{\varepsilon_{L, M}(p) - \varepsilon_{l', m'}(p)}{2r_0^2} + i\eta} \right). \quad (14)$$

In this expression, $n(l', m')$ and $n(L, M)$ denote the occupancy of the initial and final angular momentum states respectively and (l, m) represents the excitation. The quantity η is an infinitesimal damping term and $\varepsilon_{l, m}(p)$ is given by Eq. (6).

As for the integral in this expression, we will write $\Psi_{p,l'}(\Omega)$ and $\Psi_{p,L}^*(\Omega)$ explicitly by using Eq. (7) and ignore the higher order terms involving p^4 in the resulting integrand. This allows us to write the integral with five terms as

$$\begin{aligned}
& \int Y_{lm}(\Omega)\Psi_{L,M}^*(p,\Omega)\Psi_{l',m'}(p,\Omega) d\Omega = (1 + \frac{2p^4}{l'^2})^{-1/2}(1 + \frac{2p^4}{L^2})^{-1/2} \\
& \times [\int Y_{lm}(\Omega)Y_{L,M}^*(\Omega)Y_{l',m'}(\Omega) d\Omega + \int Y_{lm}(\Omega)Y_{L,M}^*(\Omega)\frac{p^2}{l'}Y_{l'+2,m'}(\Omega) d\Omega \\
& + \int Y_{lm}(\Omega)Y_{L,M}^*(\Omega)\frac{p^2}{l'}Y_{l'-2,m'}(\Omega) d\Omega + \int Y_{lm}(\Omega)\frac{p^2}{L}Y_{L+2,M}^*(\Omega)Y_{l',m'}(\Omega) d\Omega \\
& + \int Y_{lm}(\Omega)\frac{p^2}{L}Y_{L-2,M}^*(\Omega)Y_{l',m'}(\Omega) d\Omega]. \tag{15}
\end{aligned}$$

The evaluation of the integrals with three spherical harmonics is facilitated by using [21]

$$\begin{aligned}
& \int Y_{LM}^*(\Omega)Y_{l,m}(\Omega)Y_{l',m'}(\Omega) d\Omega = \sqrt{\frac{(2l+1)(2l'+1)}{4\pi(2L+1)}} \\
& \langle l'l'; 00|ll'; L0 \rangle \langle l'l'; mm'|ll'; LM \rangle. \tag{16}
\end{aligned}$$

We can now take the square of Eq. (15). All the cross-terms vanish due to the orthogonality of the Clebsch-Gordon coefficients and the end result is a sum of the squares of the five terms. To convert the Clebsch-Gordon coefficients to Wigner 3j-symbols, we use [22]

$$\begin{pmatrix} l & l' & L \\ m & m' & -M \end{pmatrix} = (-1)^{l-l'+M}(2L+1)^{-1/2} \langle l'l'; mm'|ll'; LM \rangle, \tag{17}$$

where the parenthesized (2×3) array of numbers in Eq. (17) is the Wigner 3j-symbol. This prescribes which electronic transition processes contribute to excitations of the electron gas. The value of this symbol vanishes unless $|L - l'| \leq l \leq L + l'$ and $L + l + l' = \text{even integer}$. In the nonvanishing case, if we set $l + l' + L = 2k$ ($k = \text{integer}$), the value of the squared 3j-symbol is explicitly given by

$$\begin{pmatrix} l & l' & L \\ 0 & 0 & 0 \end{pmatrix}^2 = \frac{(l' + L - l)!(L + l - l')!(l + l' - L)!}{(l' + L + l + 1)!} \times \left(\frac{p!}{(p - l')!(p - L)!(p - l)!} \right)^2. \tag{18}$$

The next task is to carry out the summations over m' and M in the Lindhard term. This is nontrivial since both the second Clebsch-Gordon coefficient and the perturbed energy eigenvalues are m' and M dependent. This necessitates an approximation. We will use $m' = l'$ and $M = l' + 1$ in the perturbed energy eigenvalues and carry out the summations

over m' and M only for the Clebsch-Gordon coefficient using the identity

$$\sum_{m'=-l'}^{l'} \sum_{M=-L'}^{L'} \begin{pmatrix} l_1 & l' & L \\ m_1 & m' & -M \end{pmatrix} \begin{pmatrix} l_2 & l' & L \\ m_2 & m' & -M \end{pmatrix} = \frac{1}{2l_1 + 1} \delta_{l_1, l_2} \delta_{m_1, m_2}. \quad (19)$$

This approximation is justified in two ways. First, it is consistent with dipole transition rules. Second, even if one prefers to choose a different initial magnetic quantum number, since the energy term has $\frac{1}{2r_0^2}$ prefactor which is on the order of 10^{-6} a.u. for the spheres' radii in the present study, it would not change the values of the resulting plasmon energies unless Fermi level is very high. We will be avoiding that regime in this paper. In essence, this approximation means that we are carrying out the summations in the regime where the difference in energy eigenvalues is quite insensitive to the magnetic quantum number dependence. Hence, according to this approximation, the energy difference $\Delta\varepsilon_{L,l'}(p) = \varepsilon_{L,l'+1}(p) - \varepsilon_{L,l'}(p)$, is given by

$$\Delta\varepsilon_{L,l'}(p) = L(L+1) - l'(l'+1) + 2p + \frac{p^2}{2} \left(\frac{(l'+1)^2}{L^2} - 1 \right) + p^2 \left(\frac{1}{L} - \frac{1}{l'} \right). \quad (20)$$

After handling the magnetic quantum number dependent Clebsch-Gordon coefficient this way and converting the other one to a Wigner 3j-symbol, the final expression for the magnetic field dependent Lindhard response function becomes

$$\begin{aligned} D_R^0(r_0, p, l, \omega) &= \sum_{l'} \sum_L n(l')(1 - n(L)) \frac{1}{4\pi} \frac{1}{1 + \frac{2p^4}{l'^2}} \frac{1}{1 + \frac{2p^4}{L^2}} \\ &\times [(2l'+1)(2L+1) \begin{pmatrix} l & l' & L \\ 0 & 0 & 0 \end{pmatrix}^2 + (2l'+1)(2L+5) \begin{pmatrix} l & l' & L+2 \\ 0 & 0 & 0 \end{pmatrix}^2 \frac{p^4}{L^2} \\ &+ (2l'-3)(2L+1) \begin{pmatrix} l & l' - 2 & L \\ 0 & 0 & 0 \end{pmatrix}^2 \frac{p^4}{l'^2} + (2l'+5)(2L+1) \begin{pmatrix} l & l' + 2 & L \\ 0 & 0 & 0 \end{pmatrix}^2 \frac{p^4}{l'^2} \\ &+ (2l'+1)(2L-3) \begin{pmatrix} l & l' & L-2 \\ 0 & 0 & 0 \end{pmatrix}^2 \frac{p^4}{L^2}] \\ &\times \left(\frac{1}{\omega - \frac{\Delta\varepsilon_{L,l'}(p)}{2r_0^2} + i\eta} - \frac{1}{\omega + \frac{\Delta\varepsilon_{L,l'}(p)}{2r_0^2} + i\eta} \right). \end{aligned} \quad (21)$$

This result is rigorous to order p^4 since second order perturbation theory in the wave function would have contributed a p^8 term. The reason why we preferred to write the final expression in terms of Wigner 3j-symbols rather than Clebsch-Gordon coefficients is that

they illuminate more clearly which terms are contributing to the summation in the Lindhard response function. This will be very crucial for the analysis in the next section. The calculation of the RPA dielectric function can be accomplished in a straightforward manner by using a Dyson series once we know the Lindhard response function given by Eq. (21). The RPA dielectric function has the form

$$\epsilon_{RPA}(r_0, p, l, \omega) = 1 - v(l, r_0)D_R^0(r_0, p, l, \omega). \quad (22)$$

III. RESULTS AND DISCUSSION

In the many-body theory of the two-dimensional homogeneous spherical electron gas, two types of excitations are possible: single particle excitations and surface plasmons. In first case, the imparted angular momentum is absorbed completely by a single electron and it gets excited to a higher angular momentum state. On the other hand, surface plasmons are waves that propagate along the surface of a conductor, usually a metal. In essence, these are light waves that are trapped on the surface because of their interaction with the free electrons of the conductor. The free electrons respond collectively by oscillating in resonance with the light wave, and this resonant interaction between the surface charge oscillation and the electromagnetic field of the light forms the surface plasmon. In both single-particle excitations and the surface plasmons, the excitation is characterized by the angular momentum l and energy ω .

Surface plasmon energies appear when the dielectric function defined by Eq. (22) satisfies the following two equations:

$$Im[\epsilon_{RPA}(r_0, p, l, \omega)] = 0 \quad (23)$$

$$Re[\epsilon_{RPA}(r_0, p, l, \omega)] = 0. \quad (24)$$

Now, the first equation brings the only condition that $\omega \neq \frac{\Delta\epsilon_{L,l}(p)}{2r_0^2}$ which means the plasmon energies lie outside the region of single-particle excitations defined by $\omega = \frac{\Delta\epsilon_{L,l}(p)}{2r_0^2}$. In order to find the values of plasmon energies, one has to solve Eq. (24) for successive values of l . In Fig. 1, we show the calculated plasmon energies in zero magnetic field ω_l as a function of l for three spheres with different radii. All spheres contain 882 electrons and $L_F=20$. As the radius gets larger, the plasmon energies decrease for each mode due to the $\frac{1}{2r_0^2}$ factor in Eq. (21).

These plasmons are the poles of the density-density correlation function and account for the case where the electrons are delocalised and their wave function spreads out over the entire sphere. On the other hand, we can also obtain plasmon modes that represent the charge density oscillations if the electrons are localised in a Wigner lattice.[23] It is possible to regard the latter case as a nanoshell with infinitesimal thickness. Nanoshells consist of a thin gold or silver shell around a dielectric core.[24, 25, 26, 27] The electronic and optical properties of metallic shell structures have been of interest in the context of atomic physics as well. A general semiclassical approach (SCA) was developed and applied to describe collective resonances in inner atomic shells of heavy atoms.[28, 29] For a spherical shell geometry with a step-function charge density, SCA predicts two collective oscillation modes for each component of angular momentum.[28] The energies of these plasmons are given by

$$\omega_{l\pm}^2 = \omega_s^2 \left[1 \pm \frac{1}{2l+1} \sqrt{1 + 4l(l+1)x^{2l+1}} \right] \quad (25)$$

where $\omega_s = \sqrt{\frac{2\pi e^2 n_0}{m_e}}$ is the surface plasmon energy and x is the aspect ratio defined as the ratio between the inner and outer radii of the metallic shell. The quantity n_0 represents the volume electron density. We will be considering only ω_{l-} in Eq. (25) since the other one lies far higher in energy spectrum and would be very difficult to detect experimentally.

If the electron layer has a thickness d on the order of a few nanometers just like the case of a multielectron bubble, we can rewrite eq. (25) as

$$\omega_{l-}^2(\nu, d, r_0) = \frac{2\pi e^2 \nu}{dm_e} \left[1 - \frac{1}{2l+1} \sqrt{1 + 4l(l+1) \left(\frac{r_0 - d}{r_0} \right)^{2l+1}} \right], \quad (26)$$

and take the limit $d \rightarrow 0$ to obtain:

$$\omega(l) = \sqrt{\frac{Ne^2 l(l+1)}{m_e r_0^3 (2l+1)}}. \quad (27)$$

This result is in perfect agreement with the plasmon dispersion relation derived by Klimin et. al. based on a simple harmonic oscillator model.[30] In Fig. 1 we also show for comparison the plasmon energies which were obtained by inserting the same parameters we used to solve Eq. (24) in Eq. (27). The difference in plasmon energies may be a useful way of probing the Wigner lattice and electron liquid phases of electrons on a spherical surface.

Throughout the rest of the paper, we will concentrate on the dipolar plasmon energy in a finite magnetic field since in the long wavelength limit light excites only this mode. This means we have to solve Eq. (24) for $l = 1$. We now determine the range over which we

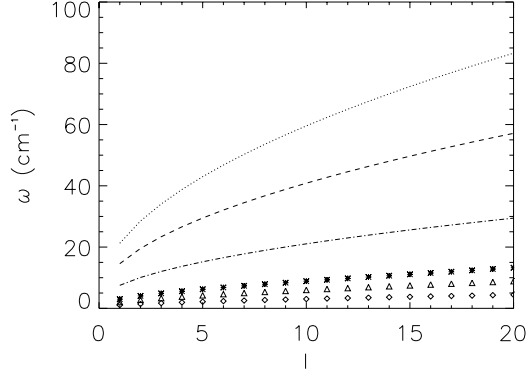


FIG. 1: This figure shows the calculated plasmon energies ω_l for the S2DEG as a function of angular momentum l in zero magnetic field. $L_F=20$ and the number of electrons is 882. The radii of the spheres are 3980 a.u. (stars), 5117 a.u. (triangles) and 7960 a.u. (diamonds). The dotted, dashed and dash-dotted lines represent the plasmon energies obtained from Eq. (27) by using these parameters respectively.

should carry out summations over initial state l' and final state L in the five 3j symbols in Eq. (21). We need to include only those terms for which Wigner 3j-symbol is not zero in each case.

We can now start considering each Wigner 3j-symbol separately. The first term which involves $\begin{pmatrix} l & l' & L \\ 0 & 0 & 0 \end{pmatrix}^2$ is the only term that survives in zero magnetic field limit where other four terms with p dependence vanish. This Wigner symbol is zero unless $|L-l'| \leq 1 \leq L+l'$ which implies l' summation for this term runs from $L_F - 1$ to L_F while L summation runs from l' to $l' + 1$. Obviously, the only allowed one-particle excitations here range from L_F to $L_F + 1$. The next two terms involve $\begin{pmatrix} l & l' & L+2 \\ 0 & 0 & 0 \end{pmatrix}^2$ and $\begin{pmatrix} l & l'-2 & L \\ 0 & 0 & 0 \end{pmatrix}^2$. They vanish unless $|L+2-l'| \leq 1 \leq L+l'+2$ and $|L-l'+2| \leq 1 \leq L+l'-2$ respectively. These inequalities can never be satisfied since final angular momentum state L is always greater than initial one l' , hence these excitations do not contribute in summations over initial and final angular momentum states.

Finally, let us consider the remaining two terms, namely those two that involve

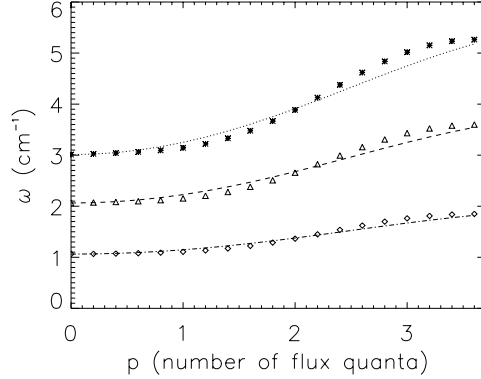


FIG. 2: This figure shows the dependence of dipolar plasmon energy on the magnetic field for three different spheres with $L_F=20$ and 882 electrons. The x-axis shows p , the number of flux quanta piercing through the sphere. The radii of the spheres are 3980 a.u. (stars), 5117 a.u. (triangles) and 7960 a.u. (diamonds). The dotted, dashed and dash-dotted lines represent the fits obtained by using Eq. (28) for these parameters respectively.

$\begin{pmatrix} l & l' + 2 & L \\ 0 & 0 & 0 \end{pmatrix}^2$ and $\begin{pmatrix} l & l' & L - 2 \\ 0 & 0 & 0 \end{pmatrix}^2$. They vanish unless $|L - l' - 2| \leq 1 \leq L + l' + 2$ and $|L - l' - 2| \leq 1 \leq L + l' - 2$ respectively. This means that the summation over l' for these terms runs from $L_F - 3$ to L_F while the summation over L runs from l' to $l' + 3$. For example, an excitation from L_F to $L_F + 3$ is allowed for these terms even though we are exciting the sphere with an $l = 1$ mode. This is a consequence of the magnetic field which introduces a coupling between $l = 1$ and $l = 3$ modes. In the absence of a magnetic field, $p = 0$ and these two terms vanish, and the $l = 1$ and $l = 3$ modes decouple.

In Fig. 2 and 3 we show the dipolar plasmon energy as a function of the number of flux quanta piercing through the sphere for three different radii to demonstrate this coupling effect. In Fig. 2, the Fermi angular momentum number is 20. As the magnetic field is increased, the dipolar plasmon energy starts increasing from its zero-field value which is just the $l = 1$ plasmon to a value somewhere between the zero-field values of ω_1 and ω_3 . For finite magnetic field, the $l = 1$ and $l = 3$ modes are coupled and as the strength of the field increases, so does the weight of the $l = 3$ contribution resulting in the increasing

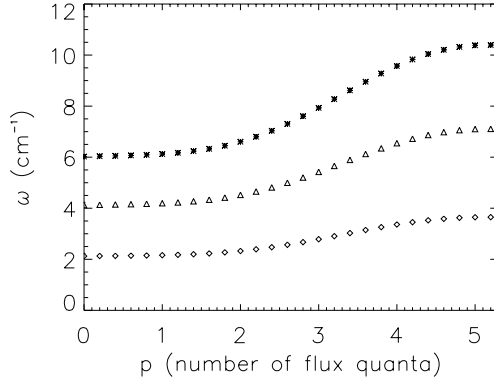


FIG. 3: This figure shows the dependence of dipolar plasmon energy on the magnetic field for three different spheres with $L_F=41$ and 3528 electrons. The x-axis shows p , the number of flux quanta piercing through the sphere. The radii of the spheres are 3980 a.u. (stars), 5117 a.u. (triangles) and 7960 a.u. (diamonds).

blue-shift of the dipolar plasmon mode as a function of the magnetic field. We should also point out that we achieve more blue-shift for the same number of flux quanta for smaller spheres. At constant p and L_F , the deviation from the zero-magnetic field plasmon energy is controlled by the multiplication factor $\frac{1}{2r_0^2}$ in Eq. (21). This factor is responsible for the smaller blue-shift for larger spheres.

Fig. 3 illustrates the effect of changing the number of electrons on the sphere while keeping the radius constant. In this figure, the Fermi angular momentum number is 41. The radii are the same as the ones we used in Fig. 2 hence surface electron densities are 4 times larger. The zero-field plasmon energies for all radii almost double compared to Fig. 2 due to the linear dependence on Fermi angular momentum number in the Lindhard response function. The plasmon energies depend on the square root of the surface charge density. In essence, these figures reveal that the function of changing radius while keeping the number of electrons constant is to shift the whole curve up or down and to reduce or increase the maximum blue-shift achieved.

The last point we have to touch upon about these figures is the strength of the magnetic field where the perturbative approach fails. We should recall the perturbed wavefunction

Eq. (7) in order to understand this. Since all excitations take place around L_F , the most strongly contributing angular momenta l are those close to L_F . This means when p^2 starts approaching L_F , the second and third terms in the perturbed wavefunction become comparable to the first one due to $\frac{p^2}{l}$ factor. In this limit, our current first order perturbative treatment fails and higher angular momentum spherical harmonics need to be included. For this reason, we only plotted our figures up until dipolar plasmon energy saturated. This corresponds to $p = 3.6$ in Fig. 2 where $L_F = 20$ and $p = 5.2$ in Fig. 3 where $L_F = 41$. Our present treatment is valid only until these p values. We believe the saturation in the dipolar plasmon energies is an artifact of first order perturbation theory and that the plasmon energies would continue to increase with p if a higher order perturbation theory was used.

Next, we will investigate the behaviour of the dipolar plasmon energy as a function of the number of electrons for constant radius and try to elucidate the nature of the mixing between different modes explicitly for a weak magnetic field. In Fig. 4 we plotted the $l = 1$ and $l = 3$ plasmon energies in zero magnetic field for a sphere of radius 3980 a.u. alongside with the dipolar plasmon energy when a uniform magnetic field of 0.029T is applied. The dipolar plasmon energy consists of an admixture of $l = 1$ and $l = 3$ modes and as the number of electrons increases the weight of the $l = 3$ mode decreases as seen from the figure. We can explain this by considering Eq. (21). The contribution of the $l = 3$ mode is contained only in the last two terms in this expression as we discussed before. Increasing the number of electrons on the sphere means increasing the Fermi angular momentum number L_F . For example, $N=4050$ and $N=10658$ correspond to $L_F=44$ and $L_F=72$ respectively in Fig. 4. This clearly implies that the initial and final angular momentum numbers l' and L also start increasing since they are close to L_F , however we keep the magnetic field and p constant. Hence the $\frac{p^4}{L^2}$ and $\frac{p^4}{l'^2}$ factors in the last two terms in Eq. (21) start decreasing as we increase the number of electrons and this reduces the weight of the $l = 3$ mode in the admixture gradually. That is why the dipolar plasmon energy in finite field approaches $l = 1$ mode as the number of electrons increase.

Finally, we will try to demonstrate the nature of the coupling between ω_1 and ω_3 modes in the presence of magnetic field by using a simple qualitative equation which has the form:

$$\omega_1(p) = \frac{\omega_1 + \frac{p^2}{L_F}\omega_3}{\sqrt{1 + \frac{p^4}{L_F^2}}}. \quad (28)$$

This equation is reminiscent of the perturbed wave functions we used in our RPA calculations

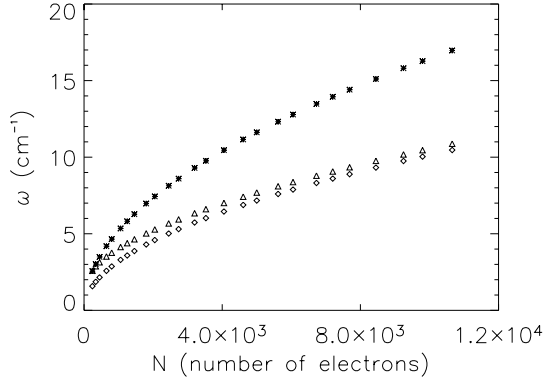


FIG. 4: This figure demonstrates the dependence of the dipolar plasmon energy on the number of electrons on the sphere. The radius is constant and 3980 a.u. Diamonds and stars denote the plasmon energies for $l = 1$ and $l = 3$ modes respectively in zero magnetic field. Triangles represent the dipolar plasmon energies when a magnetic field of 0.029T is applied on the sphere.

and phenomenologically describes the coupling of the $l = 1$ and $l = 3$ plasmons for finite magnetic field. In Fig. 2, we plotted this equation alongside with the numerically calculated plasmon energies for three spheres with different radii. $L_F=20$ and the number of electrons is 882 for all spheres. It is clear from this figure that this phenomenological equation agrees very well with the numerical data that were obtained by solving Eq. (24).

IV. CONCLUSIONS

In this paper, we investigated the optical properties of a two-dimensional electron gas constrained on a spherical surface in the presence of a weak uniform magnetic field which causes Zeeman shift in electronic energy levels. We treated this problem perturbatively within the random-phase approximation scheme. We concentrated on the behaviour of the dipolar plasmon energy in particular. We showed that there is a blue-shift in this plasmon mode compared to its zero magnetic-field value and the shift tends to increase as a function of the magnetic field. This blueshift could be explained as a magnetic field strength dependent mixing between the ω_1 and ω_3 plasmons. We also analysed the behaviour of this plasmon

mode as a function of the density of electrons on the sphere with and without the magnetic field. Further generalizations of this model for nanoshells of finite thickness are left for future studies.

Acknowledgments

This work was supported by the Robert A. Welch foundation under the grant C-1222, and by the Multi-University research Initiative of the Army Research Office. It is a pleasure to acknowledge valuable discussions with C. Dutta and computational help from C.Oubre. We are also very grateful to J. Tempere for his useful comments about the different phases of multielectron bubbles and Wigner crystallization.

-
- [1] F. Haldane, Phys. Rev. Lett. **51** (7), 605 (1983).
 - [2] G. Fano, F. Ortolani, and E. Colombo, Phys. Rev. B **34** (4), 2670 (1986).
 - [3] V.Melik-Alaverdian, N. Bonesteel, and G. Ortiz, Phys. Rev. Lett. **79** (26), 5286 (1997).
 - [4] J. Yiang and W. Su, J.Mod. Phys. B **11** (6), 707 (1997).
 - [5] E. Prodan, C. Radloff, N. Halas, and P. Nordlander, Science **302** (5644), 419 (2003).
 - [6] Y. Vlasov, V. Astratov, O. Karimov, A. Kaplyanskii, V.N.Bogomolov, and A.V.Prokofiev, Phys. Rev. B **55** (20), R13357 (1997).
 - [7] R. Averitt and N. Halas, Phys. Rev. Lett. **78** (22), 4217 (1997).
 - [8] A. Volodin, M. Khaikin, and V. Edel'man, JETP Lett. **26** (10), 543 (1977).
 - [9] U. Albrecht and P. Leiderer, Europhys. Lett. **3**, 705 (1987).
 - [10] H. Aoki and H.Suezawa, Phys. Rev. A **46** (3), R1163 (1992).
 - [11] J. Kim, I.D.Vagner, and B. Sundaram, Phys. Rev. B **46** (15), 9501 (1992).
 - [12] A. Ralko and T. Truong, J.Phys. A: Math. and General **35**, 9573 (2002).
 - [13] D. Bulaev, V. Geyler, and V. Margulis, Phys. Rev. B **62** (17), 11517 (2000).
 - [14] J. Rayleigh, Philos. Mag. **14**, 184 (1882).
 - [15] Y.Sasaki, Y. Nishina, M. Sato, and K. Okamura, Phys. Rev. B **40** (3), 1762 (1989).
 - [16] T. Inaoka, Surf. Sci. **273**, 191 (1992).
 - [17] J. Tempere, I. Silvera, and J. Devreese, Phys. Rev. B **65** (19), 195418 (2002).

- [18] D. Aristov, Phys. Rev. B **59 (9)**, 6368 (1999).
- [19] C.Flammer, *Spheroidal wave functions* (Stanford University Press, Stanford, 1957).
- [20] I. Komarov, L. Ponomarev, and S. Slavyanov, *Spheroidal and Coulomb spheroidal functions* (Nauka, Moscow, 1976).
- [21] J. Sakurai, *Modern quantum mechanics* (Addison-Wesley Co., New York, 1994).
- [22] A. Fetter and J.D.Walecka, *Quantum theory of many-particle systems* (McGraw-Hill, New York, 1971).
- [23] J. Tempere, S. Klimin, I. Silvera, and J. Devreese, Eur. Phys. J. B **32 (3)**, 329 (2003).
- [24] S. Oldenburg, R. Averitt, S. Westcott, and N. Halas, Chem. Phys. Lett. **288**, 243 (1998).
- [25] J. Jackson and N. Halas, J. Phys. Chem. B **105 (14)**, 2743 (2001).
- [26] C. Graf and A. Blaaderen, Langmuir **18 (2)**, 524 (2002).
- [27] Y. Sun, B. Mayers, and Y. Xia, Nano Lett. **2 (5)**, 481 (2002).
- [28] G. Mukhopadhyay and S. Lundqvist, Il Nuovo Cim. B **27 (1)**, 1 (1975).
- [29] E. Prodan and P. Nordlander, Nano Lett. **3 (4)**, 543 (2003).
- [30] S. Klimin, V. Fomin, J. Tempere, I. Silvera, and J. Devreese, Solid State Comm. **126 (7)**, 409 (2003).